JOURNAL OF AIRCRAFT
Vol. 32, No. 3, May–June 1995

Navier–Stokes Applications to High-Lift Airfoil Analysis

Walter O. Valarezo*
McDonnell Douglas Aerospace, Long Beach, California 90846
and
Dimitri J. Mavriplis†
NASA Langley Research Center, Hampton, Virginia 23665-5225

This article presents applications of a compressible Reynolds-averaged Navier–Stokes method to the calculation of flows about a transport-type multielement airfoil. The unstructured-mesh method used utilizes multigrid techniques for computational efficiency and includes a selection of turbulence models. The airfoil used to benchmark the computational capability is a three-element airfoil configured for landing for which extensive experimental data have been acquired both on and off the airfoil surface at high Reynolds numbers. Comparisons of computational results vs experimental data shown here include traditional airfoil performance calculations due to configuration changes. Also discussed are detailed comparisons of computational results and experimental data obtained in the flap well region to assess the applicability of existing turbulence models to the flap slot flow. Performance comparisons are conducted for configurations tested at chord Reynolds numbers of 5 × 10^6 and 9 × 10^6 and the flap well study is based on data obtained on a similar airfoil at a chord Reynolds number of 5 × 10^5.

Nomenclature

Cp = pressure coefficient
M = freestream Mach number
n/c = nondimensional coordinate normal to airfoil
OH = overhang in percent chord
Re = Reynolds number
u/U = nondimensional velocity component
x/c = nondimensional coordinate
α = angle of attack
ΔC_l = incremental lift coefficient
δ_{af} = auxiliary flap deflection
δ_f = main flap deflection
δ_s = slat deflection
η = nondimensional vertical distance from spoiler trailing edge to flap upper surface

Introduction

HIGH-LIFT aerodynamics has received considerable attention in the literature in recent years.[1–7] The emphasis has been on reporting the effects of high Reynolds numbers on high-lift performance for representative transport wing (or airfoil) designs. The effects of Reynolds number variations on the optimized rigging (nomenclature is shown in Fig. 1) of the leading- and trailing-edge devices have been shown to be substantial for the representative configurations tested.[3,4] It has become evident that computational fluid dynamic (CFD) techniques for analyzing multielement airfoil flows could play a complementary role and enable the efficient numerical exploration of performance parameters whose investigation would otherwise require enormous tunnel occupancy. If the primary goal of any CFD method is to supplement laborious and expensive wind-tunnel testing, then high-lift analysis may be the most suitable application yet in transport aircraft development.

It is within this framework that this article is offered. Knowing the capabilities and limitations of current methods should also aid in defining future method developments. It seems appropriate to suggest minimum requirements for high-lift airfoil computations. These requirements should not be arbitrary and should mirror what is expected from a wind-tunnel test. To be useful in engineering activities, the computational method should be able to 1) reliably compute surface pressures, including separated flow regions; 2) predict lift curve up to and including maximum lift; and 3) predict airfoil performance increments due to component gap, overhang, and deflection variations.

While these may constitute a rather simple set of requirements (e.g., drag was not mentioned), the multielement airfoil problem is so complex that achieving these three requirements has proven a formidable task. Defining features of multielement airfoil flows include different transition characteristics on each of the elements,[8] merging wake/boundary layers, and separated flow regions.

This article utilizes a recently developed[9] unstructured-mesh compressible Navier–Stokes method to demonstrate current capability. The experimental data used for the comparisons

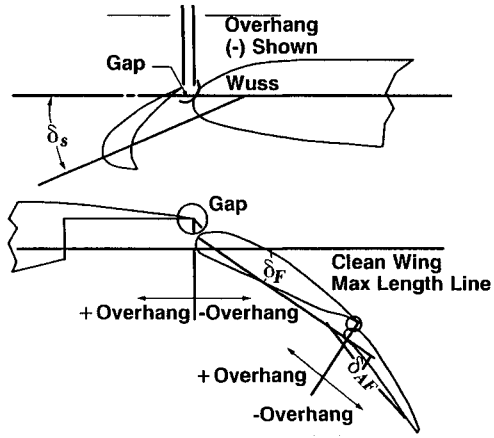

Fig. 1 Multielement airfoil nomenclature.

Presented as Paper 93-3534 at the AIAA Applied Aerodynamics Conference, Monterey, CA, June 20–23, 1993; received Aug. 30, 1993; revision received Oct. 15, 1994; accepted for publication Oct. 20, 1994.

*Principal Specialist, Aerodynamics Technology; currently, Principal Engineer, Aerodynamics, Boeing Commercial Airplane Group, P.O. Box 3707, Seattle, WA 98124-2207. Senior Member AIAA.

†Senior Staff Scientist, Institute for Computer Applications in Science and Engineering. Member AIAA.

is that of Ref. 7. Computations will be shown for performance effects due to gap variations and changes in Reynolds numbers. Comparisons will also be shown with steady flowfield data.[10] Also shown are comparisons of computational results obtained in the flap well region of the airfoil with experimental results obtained using a laser Doppler velocimetry (LDV) system.[11] The measurements of Ref. 11 (while obtained at only 5×10^5 Reynolds number) indicated substantial differences in the development of the separated flow bubble in the flap well due to flap gap variations. Hence, this database represents a useful preliminary evaluation tool for existing computational methods and turbulence models in particular. Finally, grid density effects shown here were computed after simply increasing mesh sizes of existing coarser grids without additional manual enrichment of areas such as the slat and flap well, since the authors felt this would not be practical in a daily use mode.

Description of Numerical Approach

The computational technique is based on an unstructured grid approach. Unstructured grids provide a flexible way of dealing with complex geometries, such as close-coupled multielement airfoil configurations. The use of adaptive meshing, which the authors expect to ultimately be essential for accurately resolving complex viscous flows, can also be relatively easily incorporated in the context of unstructured meshes.[12]

The flow solution technique is based on a Galerkin finite element discretization, where the flow variables are assumed to vary linearly over the triangular elements on the mesh.[13] Additional artificial dissipation is added as a blend of a Laplacian and biharmonic operator to capture shocks and maintain stability in smooth regions of the flow, respectively. Convergence to steady state is accelerated using an unstructured multigrid algorithm that relies on a sequence of independent coarse meshes. Each multigrid iteration involves a sequence

	Geometry A	Geometry B
Slat Deflection	-30°	-30°
Slat Gap	2.95%	2.95%
Slat Overhang	-2.5%	-2.5%
Flap Deflection	30°	30°
Flap Gap	1.27%	1.5%
Flap Overhang	0.25%	0.25%

Fig. 2 Slat and flap rigging.

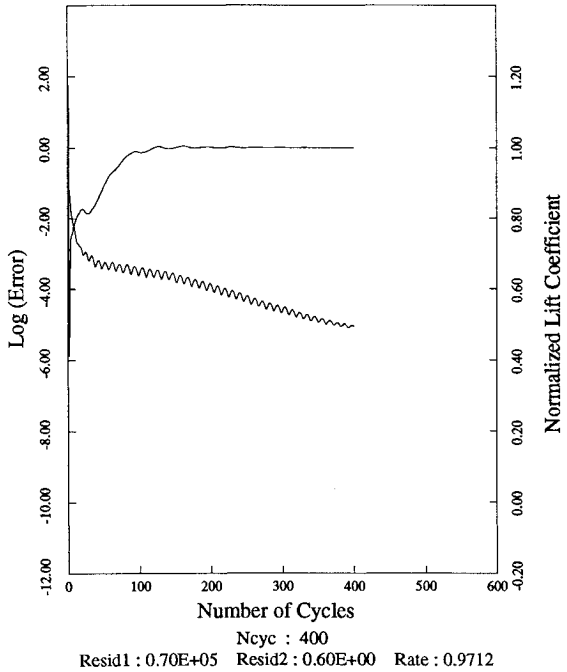

Fig. 3 Typical convergence for fine mesh case.

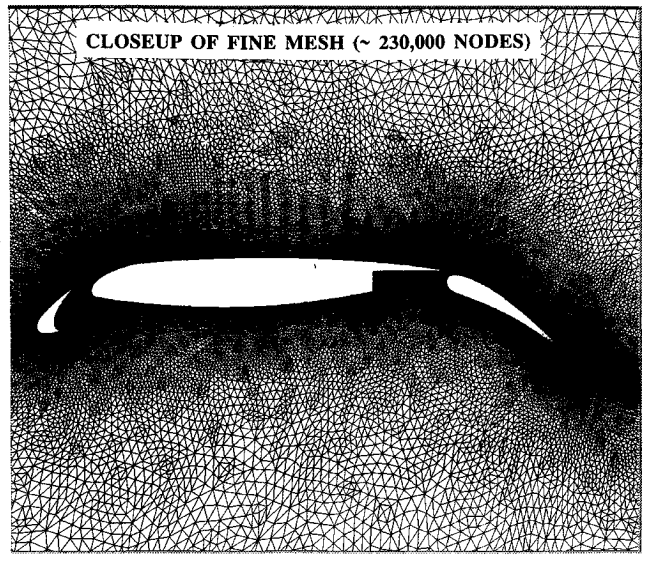

Fig. 4 Grid for three-element airfoil.

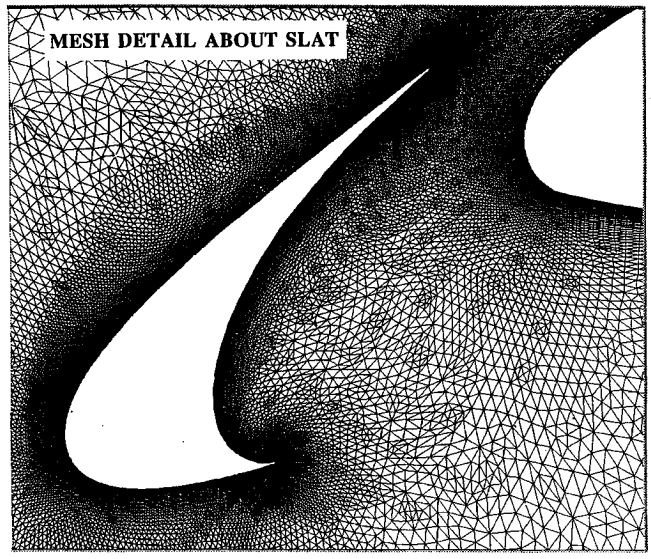

Fig. 5 Resolution of leading-edge geometry.

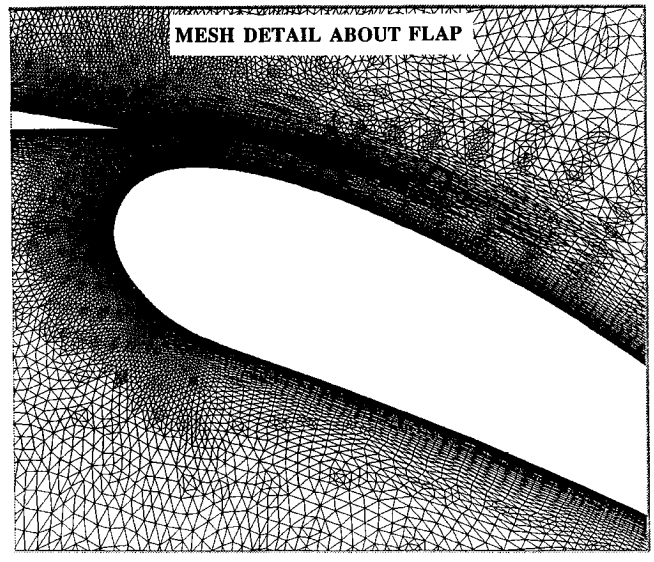

Fig. 6 Resolution of trailing-edge geometry.

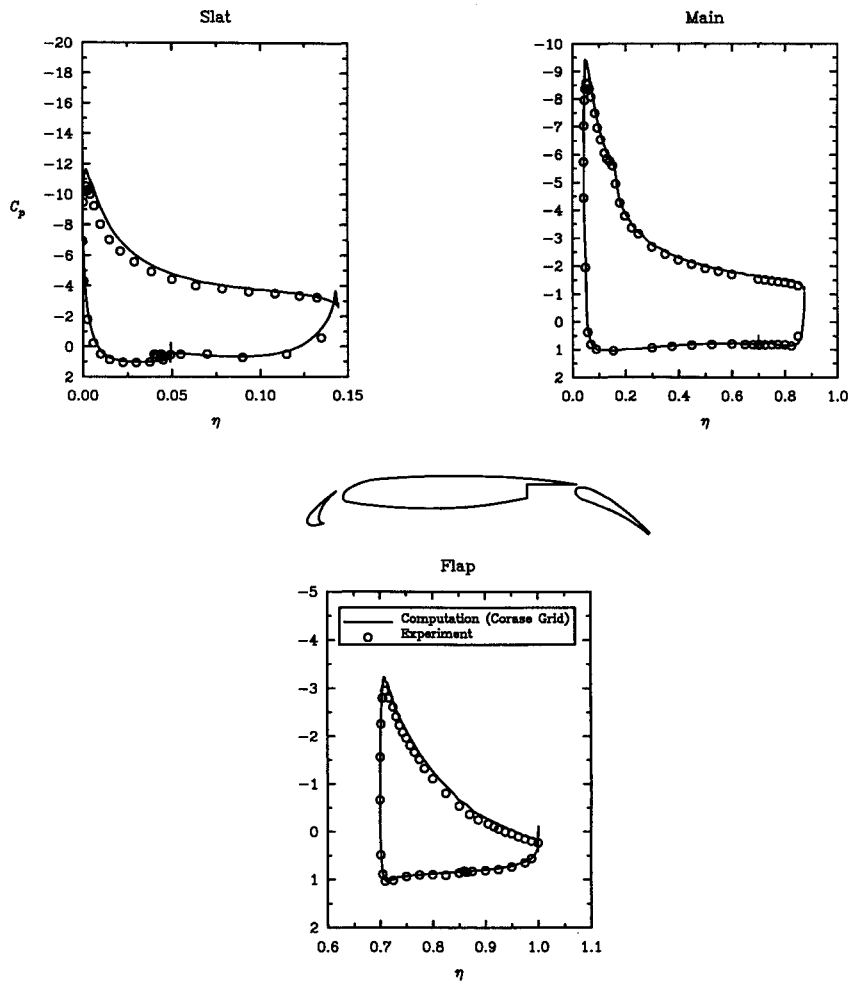

Fig. 7 Surface pressure comparison at α = 16 deg.

on time steps that begins on the fine mesh and visits each coarser mesh until the coarsest mesh is reached, at which point the corrections are interpolated back to the finest grid, and a new iteration is initiated. The multigrid procedure yields a convergence rate that is independent of the mesh size, and typically results in an order of magnitude increase in solution efficiency.[13,14]

A number of turbulence models have been implemented. These include the one-equation models of Baldwin and Barth,[15] Spalart and Allmaras,[16] and the two-equation k-ε model, either using wall functions or integrated up to the wall.[9] The turbulence equations are solved simultaneously, but decoupled from the flow equations. The convergence of the turbulent equations is accelerated using the unstructured multigrid technique, thus ensuring similar convergence rates for the flow and turbulent equations, and improving the overall efficiency of the solver.

Effort has been expended in building an efficient and practical analysis capability for two-dimensional flows. The grid generation phase involves an interactive preprocessor that enables splining of the geometry and determination of the mesh point density. Journaling is available to facilitate the generation of multiple coarse grids for the multigrid algorithm, and for regenerating grids about geometries with small changes (such as flap gap studies). A simple edge-based datastructure is employed for all operations in the flow solver, greatly reducing the memory overhead traditionally associated with unstructured grids, and accelerating the computational rates.

All preprocessing is performed directly in the initial stages of the flow solver, including the intergrid interpolation for the multigrid algorithm. All such operations require an insignificant fraction of the total solution time. The flow solver requires about 150 words per grid point, and convergence can normally be obtained in 200–400 cycles (four significant figures in lift coefficient, or four orders of magnitude decrease in the residual). Thus, a typical grid for a three-element airfoil (about 50,000 points) requires 8 MWords of memory and 17 min of CPU time on a single processor of the Cray Y-MP-C90, or 60 Mbytes of memory (double precision) and 10 h of CPU time on an IRIS Indigo R4000 workstation. When performing multiple analysis runs on the same geometry (lift curve generation), the solution time can be cut in half by using the solution of the previous run as the initial condition for the subsequent case. The CPU estimates given here are intended to be representative, but the reader should note that these times can fluctuate considerably depending on how close the elements of the airfoil are to each other, which turbulence model is specified, and the overall grid density.

Performance Calculations

Computations were conducted for an advanced three-element airfoil configured for landing. The flap was tested at two different gaps to provide a database for CFD calibration (Fig. 2). The two cases will be referred to as geometries A and B, respectively. A typical convergence history for the finest mesh used (~230,000 nodes) is shown in Fig. 3. A closeup of the fine mesh and details about the slat and flap are shown in Figs. 4–6, respectively.

All computations shown in this section were performed using the Spalart–Allmaras model. Results are shown in Fig. 7 for geometry A. Excellent agreement is seen with the experimental data[7] at this condition (Mach 0.2 and 9×10^6

Reynolds number). However, the integrated lift results of Fig. 8 are seen to overpredict lift at all angles of attack. While the good agreement of surface pressures but not-so-good correlation on lift may appear discouraging, it is important to recognize that computational methods can be very useful if trends can be predicted accurately. Absolute predictions are often difficult to obtain because of inaccuracies in the analysis tools and/or the database itself.

The results of Fig. 9 show that the present method captures the effect of Reynolds number on lift. The fine mesh computations correctly capture the increased lift occurring at 9×10^6 Reynolds number compared to 5×10^6. It can be seen that the coarse mesh computations would have misrepresented the trend near the stall angle of attack. These results suggest that high levels of grid density may be required to reliably capture small but important performance increments. Results are shown for geometry B in Fig. 10. Changes in lift performance due to flap gap (B-A) are more accurately captured by using the fine mesh. Hence, small changes in performance due to Reynolds number or flap gap variations are captured quite well when the fine mesh is used.

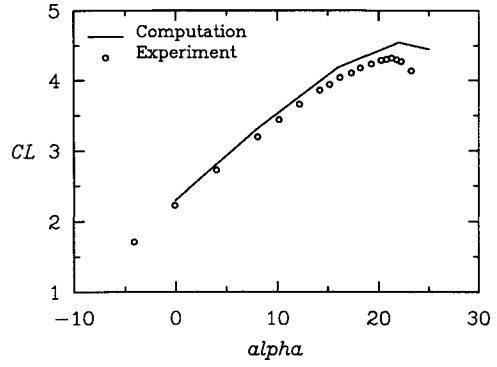

Fig. 8 Lift curve for geometry A (coarse mesh).

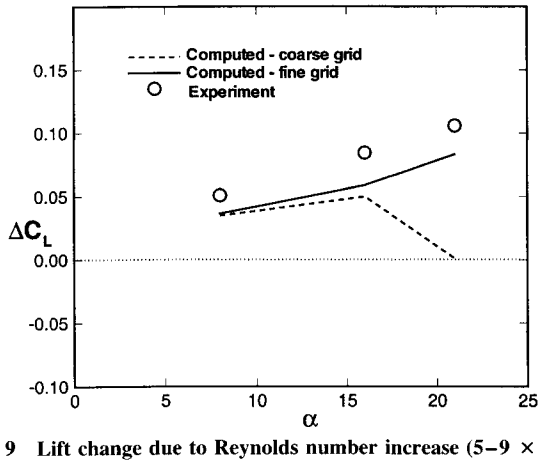

Fig. 9 Lift change due to Reynolds number increase ($5-9 \times 10^6$).

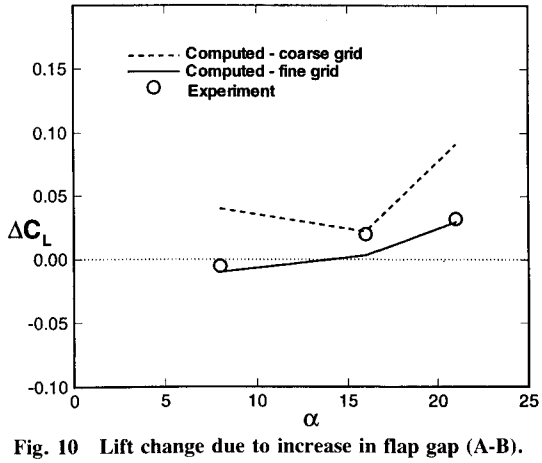

Fig. 10 Lift change due to increase in flap gap (A-B).

The flowfield data of Ref. 10 was utilized to evaluate predictive capabilities in the airfoil suction region. The comparisons of Fig. 11 show relatively good numerical prediction of the slat and main wake profiles at the specified streamwise stations for both the coarse grid and the fine grid at two values of the dissipation parameter (0.5 and 0.05). At these flow conditions ($\alpha = 8.12$ deg, 5×10^6 Reynolds number) the wakes propagate relatively close to the neighboring airfoil surfaces, in regions where appreciable grid density exists. Figure 12 represents a more demanding case. The streamwise stations are now further downstream and the flow conditions ($\alpha = 16.21$ deg, 9×10^6 Reynolds number) produce wakes that propagate further away from the airfoil surfaces in regions where the grid is considerably coarser. In this case, the numerical prediction is seen to be overly diffusive, and a combination of finer mesh density and/or lower numerical dissipation is required to capture the multiple wakes. It is conjectured that increased mesh resolution, possibly through the use of adaptive meshing, and lower dissipation rates will be required to consistently and accurately capture the detail of a multiple wake structure.

Flap Well Computations

Calculations were performed for a three-element geometry wind tunnel tested at a Reynolds number of 5×10^5 (Ref.

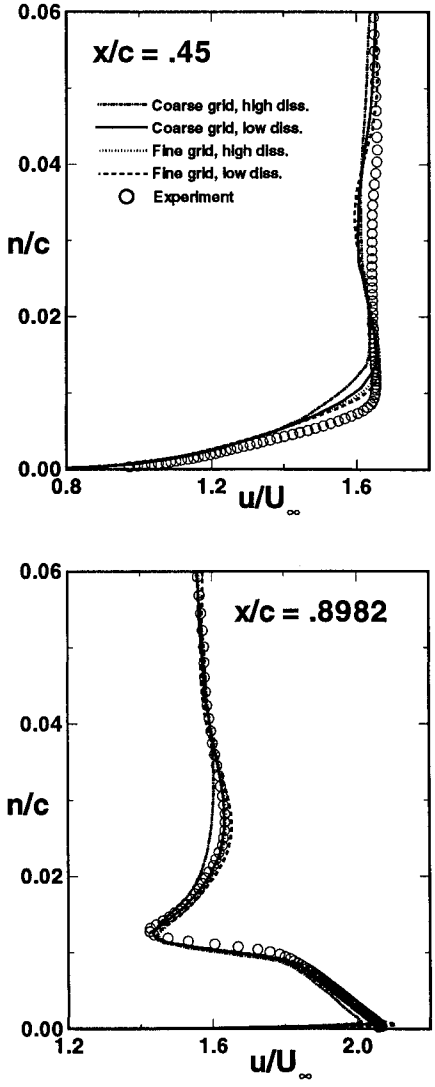

Fig. 11 Velocity profiles at $\alpha = 8.12$ deg, $Re = 5 \times 10^6$.

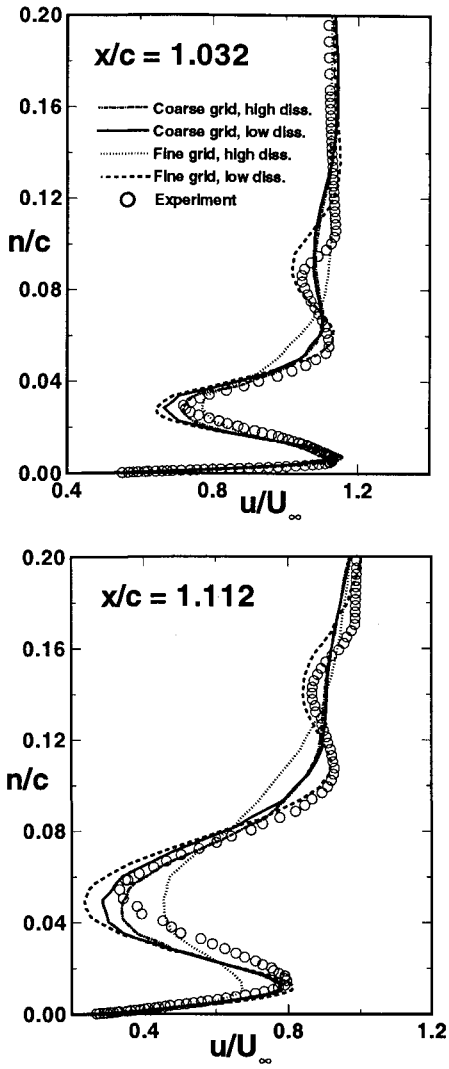

Fig. 12 Velocity profiles at $\alpha = 16.21$ deg, $Re = 9 \times 10^6$.

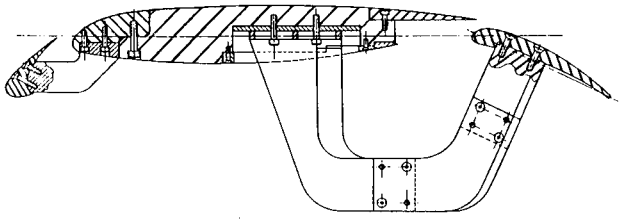

Fig. 13 Sketch of geometry.

11, Fig. 13). The model brackets were designed to provide relatively unobstructed flow (and visibility) in the flap well. The airfoil geometry is identical to geometry A with the exception of the nose region of the flap. Both the slat and flap were rigged at a 30-deg deflection.

A flap gap study was experimentally conducted and detailed flow measurements were obtained for flap gaps of 1, 2, and 3% at a fixed overhang. A closeup of the mesh utilized for the 1% gap case is shown in Fig. 14. It was desired to better understand the applicability of several turbulence models to the flap slot flow problem. Three popular turbulence models were utilized: 1) Spalart–Allmaras, 2) Baldwin–Barth, and 3) k-ε integrated up to the wall.[9] Most of the computations were performed all turbulent, with the exception of a case where the lower surface of the main element was specified to be laminar to examine any difference in the computed slot flow. Since the slot flow impacts the surface pressure development over the flap, it is anticipated that the ability to accurately predict the slot flow will manifest itself in improved performance prediction.

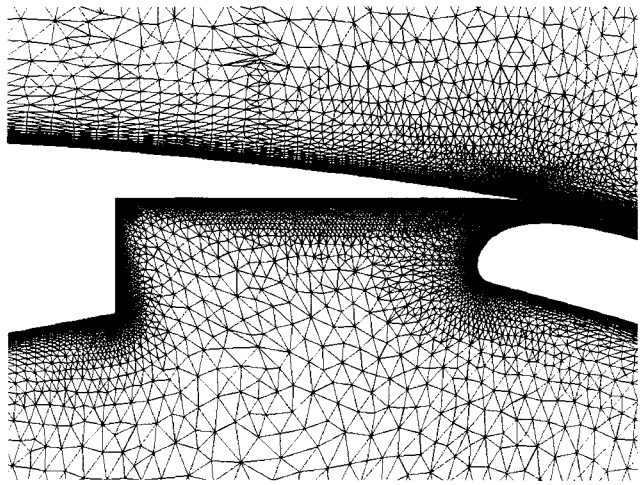

Fig. 14 Closeup of mesh for 1% gap case (~60,000 nodes).

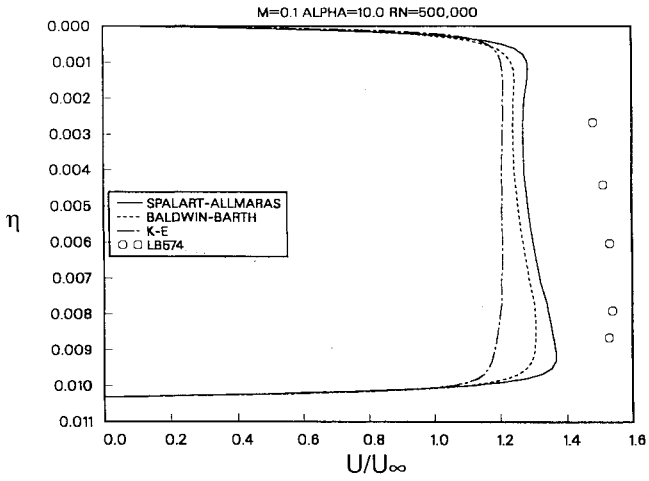

Fig. 15 Velocity through slot, 1% gap case.

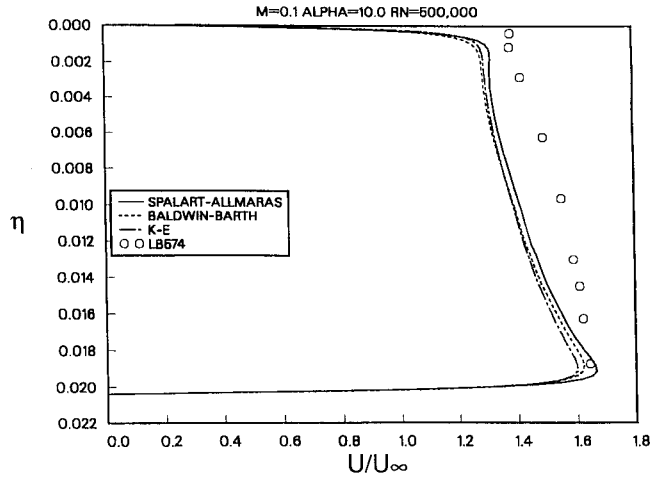

Fig. 16 Velocity through slot, 2% gap case.

Results are shown in Fig. 15 for the 1% gap case. These velocities occur in the channel between the spoiler trailing edge and the flap upper surface. These results indicate errors exceeding 20% in velocity, with use of the Spalart–Allmaras model leading to the best correlation. Computations for the

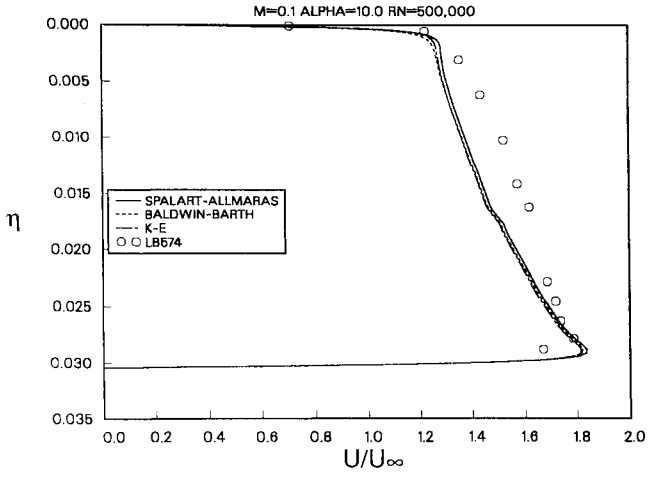

Fig. 17 Velocity through slot, 3% gap case.

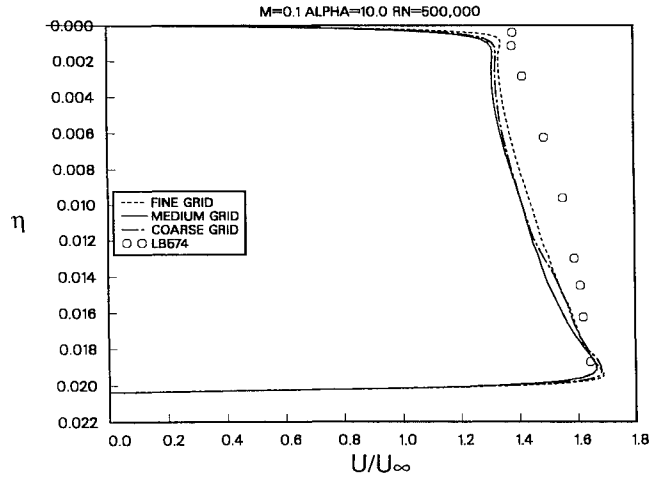

Fig. 18 Grid density effects on slot flow, 2% gap case.

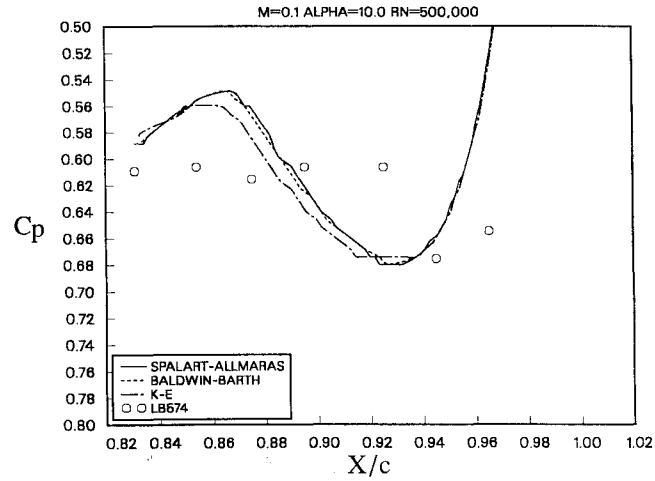

Fig. 19 Pressure distribution on spoiler lower surface (2% gap case).

2% flap gap case show improved correlation with the experimental results with the best comparison still obtained using the Spalart–Allmaras model (Fig. 16). The overall correlation with experiment is further improved at a gap of 3% (Fig. 17). It is evident that the numerical results best represented the measured data at the larger flap gaps. A grid density study was performed using the Spalart–Allmaras turbulence model to determine the sensitivity of the solution to grid changes and help establish a confidence level in the above findings. These results are shown in Fig. 18 and indicate a level of improvement due to using the fine mesh (233,068 nodes) of the same order of magnitude as that obtained by using one turbulence model over another.

Comparisons to experimental data on the spoiler lower surface were also made for completeness. Surface pressure comparisons here are useful because they can reveal if the bubble attachment point is correctly captured. Similar results were obtained for all three gap cases, only the 2% gap case is shown (Fig. 19). The method predicts pressure gradients not evident from the experimental data and the attachment point for the bubble is underpredicted by about 2% of chord. All turbulence models lead to essentially identical results. Refinement of the grid led to marginally improved prediction of the attachment location, but the overall shape of the pressure distribution in the region remained unimproved (coarse ~48,000 nodes, medium ~58,000 nodes, and fine ~250,000 nodes). Hence, there was no strong evidence that the solution could be significantly improved by using very fine grid resolution in this region. However, this result is suggestive of the need for improved turbulence modeling or additional grid resolution in other areas of the flowfield that may condition the flow physics in the flap well region.

Conclusions

This article has presented applications of a Reynolds-averaged Navier–Stokes method to multielement airfoils. The cases shown have demonstrated the usability of such a method to capture performance increments due to rigging changes and Reynolds number effects. Although qualitative results for such increments can generally be obtained with meshes of the order of 50,000 points, a fine mesh of 250,000 points is required for reliable quantitative predictions. This suggests that grid adaptation must be seriously considered for extensions to three-dimensional flows. It was found that the method yielded reasonable predictions of the flow in the flap slot, however, the location of the attachment point was underpredicted. Further grid refinement—without grid adaptation—did not appreciably change this last result.

References

[1]Fiddes, S. P., Kirby, D. A., Woodward, D. S., and Peckham, D. H., "Investigations into the Effects of Scale and Compressibility on Lift and Drag in the RAE 5m Pressurized Low-Speed Wind Tunnel," *Aeronautical Journal*, Vol. 89, Paper 1302, March 1985, pp. 93–108.

[2]Kirkpatrick, D., and Woodward, D., "Priorities for High-Lift Testing in the 1900's," AIAA Paper 90-1413, June 1990.

[3]Valarezo, W. O., Dominik, C. J., McGhee, R. J., Goodman, W. L., and Paschal, K. B., "Multielement Airfoil Optimization for Maximum Lift at High Reynolds Numbers," AIAA Paper 91-3332, Sept. 1991.

[4]Valarezo, W. O., Dominik, C. J., and McGhee, R. J., "Reynolds and Mach Number Effects on Multielement Airfoils," *Proceedings of the Fifth Symposium on Numerical and Physical Aspects of Aerodynamic Flows*, California State Univ., Long Beach, CA, Jan. 1992.

[5]Yip, L. P., Vijgen, P. M. H. W., Hardin, J. D., and Van Dam, C. P., "Subsonic High-Lift Flight Research on the NASA Transport Systems Research Vehicle (TSRV)," AIAA Paper 92-4103, Aug. 1992.

[6]Yip, L. P., Vijgen, P. M. H. W., and Hardin, J. D., "In-Flight Surface-Flow Measurements on a Subsonic Transport High-Lift Flap System," International Council of the Aeronautical Sciences, ICAS Paper 92-3.7.3, Beijing, PRC, Sept. 1992.

[7]Valarezo, W. O., Dominik, C. J., McGhee, R. J., and Goodman, W. L., "High Reynolds Number Configuration Development of a High-Lift Airfoil," *Proceedings of AGARD Conference on High-Lift Aerodynamics*, Paper 10, Banff, Canada, Oct. 1992.

[8]Nakayama, A., Stack, J., Lin, J., and Valarezo, W., "Surface Hot-Film Technique for Measurements of Transition, Separation, and Reattachment Points," AIAA Paper 93-2918, July 1993.

[9]Mavriplis, D. J., and Martinelli, L., "Multigrid Solution of Compressible Turbulent Flow on Unstructured Meshes Using a Two-Equation Model," AIAA Paper 91-0237, Jan. 1991.

[10]Chin, V. D., Peters, D. W., Spaid, F. W., and McGhee, R. J.,

"Flowfield Measurements About a Multielement Airfoil at High Reynolds Numbers," AIAA Paper 93-3137, Orlando, FL, July 1993.

[11]Nakayama, A., "An Experimental Investigation of a Flow Around the Flap Well of a Multielement Airfoil," McDonnell Douglas Rept. MDC K4310, March 1990.

[12]Mavriplis, D. J., "Turbulent Flow Calculations Using Unstructured and Adaptive Meshes," *International Journal of Numerical Methods in Fluids*, Vol. 13, No. 9, 1991, pp. 1131–1152.

[13]Mavriplis, D. J., Jameson, A., and Martinelli, L., "Multigrid Solution of the Navier-Stokes Equations on Triangular Meshes," AIAA Paper 89-0120, Jan. 1989.

[14]Mavriplis, D. J., "Three Dimensional Unstructured Multigrid for the Euler Equations," *AIAA Journal*, Vol. 30, No. 7, 1992, pp. 1753–1761.

[15]Spalart, P. R., and Allmaras, S. R., "A One-Equation Turbulence Model for Aerodynamic Flows," AIAA Paper 92-0439, Jan. 1992.

[16]Baldwin, B., and Barth, T., "A One-Equation Turbulence Transport Model for High Reynolds Number Wall-Bounded Flows," AIAA Paper 91-0610, Jan. 1991.